Mechanical behavior and apparent stiffness of flax, hemp and nettle fibers under single fiber transverse compression tests

Jason Govilas, Anouk Chevallier, Wajih Akleh, Johnny Beaugrand, Cédric Clévy, Vincent Placet

Composites: Part A 185 (2024) 108321

Contents lists available at ScienceDirect

Composites Part A

journal homepage: www.elsevier.com/locate/compositesa

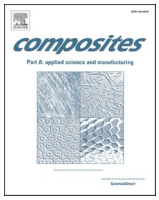

Mechanical behavior and apparent stiffness of flax, hemp and nettle fibers under single fiber transverse compression tests

Jason Govilas [a], Anouk Chevallier [a], Wajih Akleh [a], Johnny Beaugrand [b], Cédric Clévy [a], Vincent Placet [a,*]

[a] Université de Franche-Comté, CNRS, Institut FEMTO-ST, 25000 Besançon, France
[b] INRAE, UR 1268 BIA Biopolymères Interactions Assemblages, 44316 Nantes, France

ARTICLE INFO

Keywords:
Natural fibers
Elasticity
Finite element analysis (FEA)
Mechanical test

ABSTRACT

While plant fibers find extensive use across numerous applications, their transverse behavior and mechanical properties lack direct and fiber-scale characterization, posing a significant knowledge gap. This paper investigates, for the first time, the transverse behavior of flax, hemp and nettle fibers through Single Fiber Transverse Compression Tests (SFTCTs). Finite element analysis is used to study the influence of time-dependent and irreversible inelastic behavior on the fiber's response and identify configurations fit for the identification of apparent elastic properties. SFTCTs are performed experimentally with a repeated progressive loading protocol using a custom micro-mechatronic setup. An apparent fiber transverse elastic modulus of 1 to 3 GPa is identified by inverse method for all tested fibers, demonstrating high fiber anisotropy. Important inelastic features are also observed on fiber behavior. Their origin is discussed with both material behavior and structural mechanisms such as lumen collapse, identified as the main potential causes.

1. Introduction

The use of plant fibers as a composite reinforcements has gained increased popularity for its environmental, mechanical and cost benefits [1]. Bast fibers which grow on the perimeter of the plant's stem to provide structural stability, are often preferred for their higher mechanical properties [2]. While Plant Fiber Composites (PFCs) are used in a variety of applications, they are still predominantly limited to non or semi-structural roles [3]. Accurate knowledge of plant fiber mechanical properties is crucial to optimize PFC performance and expand their use to more applications.

Plant fiber mechanical properties can be obtained by direct testing at the elementary fiber scale or indirectly through composite, stem, or bundle-scale characterization [1]. While indirect methods are often easier to perform experimentally, they introduce a series of uncertainties related to the modeling of all constituents and their interactions [4]. Direct characterization at the fiber scale reduces these uncertainties [4], it is however challenging due to the complex morphology and small size of plant fibers, which are typically a few mm in length and a few tens of μm in diameter.

The vast majority of direct characterization efforts consist of tensile testing, providing the tensile properties of a wide variety of plant fibers, notably bast fibers, under various loading conditions [1]. In contrast, to the authors knowledge, no such works exist for transverse characterization. It is only by indirect testing at the composite scale that a flax fiber transverse elasticity modulus has been estimated at around 8 GPa by Baley et al. [5]. Nevertheless, fiber transverse properties play an important role in composite behavior under many typical loading cases, such as compression or bending. Significant transverse stresses are also applied to the plant fibers during fiber processing, such as hackling and scutching [1] or during the composite's compression molding [6]. The lack of knowledge on plant fiber transverse mechanical properties is thus a critical bottleneck in the prediction of PFC behavior, hindering their expansion into new applications.

The established way to study a fiber's transverse behavior is the Single Fiber Transverse Compression Test (SFTCT). The test consists of compressing the fiber transversely between a fixed and a mobile platen. It has been extensively used to identify the transverse properties of synthetic fibers such as carbon [7–9], aramid [7,10–15] and other polymer fibers [10,16–19]. Mikczinski et al. [20] studied the change in the mechanical behavior of pine and spruce wood fibers under repeated small amplitude transverse loading (1.2 mN at maximum), but did not

* Corresponding author.
E-mail address: vincent.placet@univ-fcomte.fr (V. Placet).

https://doi.org/10.1016/j.compositesa.2024.108321
Received 18 March 2024; Received in revised form 31 May 2024; Accepted 16 June 2024
Available online 17 June 2024

identify the fiber mechanical properties. To the authors knowledge, this constitutes the only example of plant fiber transverse compression in the open literature.

Contrary to tensile tests, the presence of contact between the fibers and the platens in SFTCTs, results in a non-linear fiber behavior, even if the fiber is considered purely elastic. For this reason, fiber transverse property identification, notably of the transverse elastic modulus E_T, is made by inverse method using SFTCT analytical models. The most popular of these models is the one developed by Jawad et al. [16]. It considers the fiber as a purely elastic and transversely isotropic right circular cylinder. While these assumptions reasonably represent synthetic fibers, the nature of plant fibers is significantly more complex.

Plant fibers possess intricate multilayered structures [1] that exhibit important inelastic behavior [21]. They are morphologically complex objects with intricate cross sections consisting of an exterior fiber cell wall and a central porosity, the lumen [22]. Consequently, when using SFTCT analytical models in the identification procedure, an apparent transverse elastic modulus is identified that accounts for potential structural effects related to the fiber geometry and material effects related to fiber inelasticity. Understanding the impact of these structural and material mechanisms on SFTCT results is critical to assure the relevance of the identified transverse elastic modulus. The effect of fiber geometry on the value of the identified E_T has been treated separately by our team with Finite Element Analysis (FEA) [23]. Regarding fiber inelastic behavior, Finite Element Models (FEMs) integrating plastic behavior have been used to identify yield stresses and study irreversible behavior on synthetic fiber SFTCTs [13,14,17,24,25]. However, to the authors' knowledge, no comprehensive investigation has examined the influence of ireversible or time-dependent phenomena on a fiber's response under SFTCT.

In this paper, two-dimensional (2D) FEMs of SFTCTs are used to examine how fiber wall behavior that deviates from purely-elastic, influences the fiber's response under transverse loading. Viscoelastic and elastoplastic models are utilized to examine time-dependent and irreversible mechanisms, respectively. The insights gained from these studies provide guidelines for the loading protocol and analysis of SFTCTs to achieve a fiber response that is as close to purely elastic as possible. By minimizing the influence of fiber inelastic behavior, the accuracy of the identified apparent transverse elastic modulus is enhanced. With this foundation, a custom micro-mechatronic SFTCT setup is employed to identify, for the first time, an apparent transverse elastic modulus for the three most commonly used bast fibers in Europe for composite applications: flax, hemp and nettle [1]. Kevlar ® 29 (K29) fibers are tested as a reference synthetic material for comparison purposes.

2. Materials and methods

2.1. Fiber choice preparation and dimensional analysis

Flax fibers are extracted from non-woven FlaxTape™ reinforcements (EcoTechnilin Valliquerville, France). Hemp fibers (2018 roving) were obtained through the European Union's SSUCHY project (https://www.ssuchy.eu) while nettle fibers (Roville variety) were sourced by the SusCrop- ERA-NET, NETFIB project (https://www.netfib.eu). Aramid fibers (K29), whose transverse properties have been reported in the literature [7,10,11,13], are also tested as a reference synthetic material. The aramid fibers were provided by the Ecole des Mines de Paris – Université PSL.

All plant fibers tested for the purpose of this study are isolated manually. Their ends are mounted on two separate one-part plastic tabs (Diastron Ltd. Hampshire, UK) using a photo-curing glue (DYMAX, 3099, GmbH, Wiesbaden, Germany). The inter-tab distance is of 12 mm. The samples are then mounted on a Fiber Dimensional Analysis System (FDAS) by Diastron Ltd. (Hampshire, UK) where their transverse dimensions were measured by laser scanning [26]. Three successive scans, on 27 sections regularly spaced on a 3 mm segment at the fiber's center are performed for each fiber. Using the machine's quick scanning option, a maximum and minimum apparent fiber diameter is given for each scan. An average value across all scans provides a mean minimum and maximum diameter value for each fiber.

In the case of K29 fibers, their light diffraction properties prevent the use of the FDAS system [27]. For this reason, only one end of the K29 fibers is glued on a tab and apparent diameter measurements are performed in a Scanning Electron Microscope (SEM). Due to the measurement method and the more uniform geometry of K29 fibers, a single average diameter value is calculated for each fiber.

5 fibers of each type (flax, hemp, nettle and K29) are isolated and measured. The average diameter values for each fiber type are given in Table 1. Finally, plant fibers are cut at their center, using a custom guillotine-like setup to obtain a free, straight edge. This free fiber edge can be observed during testing when placed at the edge of the lower compression platen, as seen in Fig. 1

2.2. Fiber experimental testing

2.2.1. SFTCT experimental setup

A micro-mechatronic experimental setup developed by our team for SFTCTs is used to test the fibers. The setup has been presented in [28]. Its originality lies in the replacement of a conventional upper compression platen with a custom sensor, microfabricated from a silicon wafer using Deep Reactive Ion Etching (DRIE) [29]. The sensor allows for a parallel measurement of the applied force and fiber displacement through the tracking of fiducial markers which are printed on it through photolithography. Measurements are performed in direct contact with the fiber eliminating system compliance issues. Fiber compression is controlled through the movement of the sensor using a closed loop-controlled nanopositioning stage (PIHERA 629.1, Physik Instrumente, Karlsruhe, Germany). The design, operation, calibration and performance of the used sensor are presented in [30]. The fiber is compressed by the sensor's tip on a length of 300 μm on its free extremity. The tip's roughness was measured at 57 nm through optical metrology. The parallelism between this sensor and the lower compression platen is also assured through a rotary actuator and a custom protocol with a precision under 0.1° [28]. Two microscopes allow the observation of the fiber under compression along its longitudinal and transverse section (see Fig. 1). Component control and data acquisition are performed using SIMULINK (Mathworks, Natick, USA).

The experimental setup is contained within a custom chamber with a total volume of 200 L. A control of the Relative Humidity (RH) within this enclosure is performed with a RH generator (HumiSys HF, InstruQuest Inc., Boca Raton, USA) with a flow of 20 L/min. Temperature and humidity sensors placed close to the fiber enable active RH regulation. Relative humidity inside the chamber is maintained at 50%. No active temperature regulation has been implemented. All setup components are turned on during the RH regulation stage, in order for thermal variations linked to component heating to stabilize. Tests are performed after approximately 45 min, when both RH and temperature have stabilized.

Table 1
Average apparent diameter for each fiber type. For plant fibers, where measurements are made through the FDAS, an average minimum diameter, D_{min}, and an average maximum diameter, D_{max}, are given. An average global diameter, D, is given for K29 fiber, measured through SEM imagery.

	Kevlar®29	Nettle	Hemp	Flax
D_{min}(μm)	–	13.4 ± 2.0	13.0 ± 1.8	9.8 ± 1.5
D_{max}(μm)	–	41.1 ± 5.6	23.4 ± 2.8	18.5 ± 3.5
D(μm)	11.1 ± 0.8	–	–	–

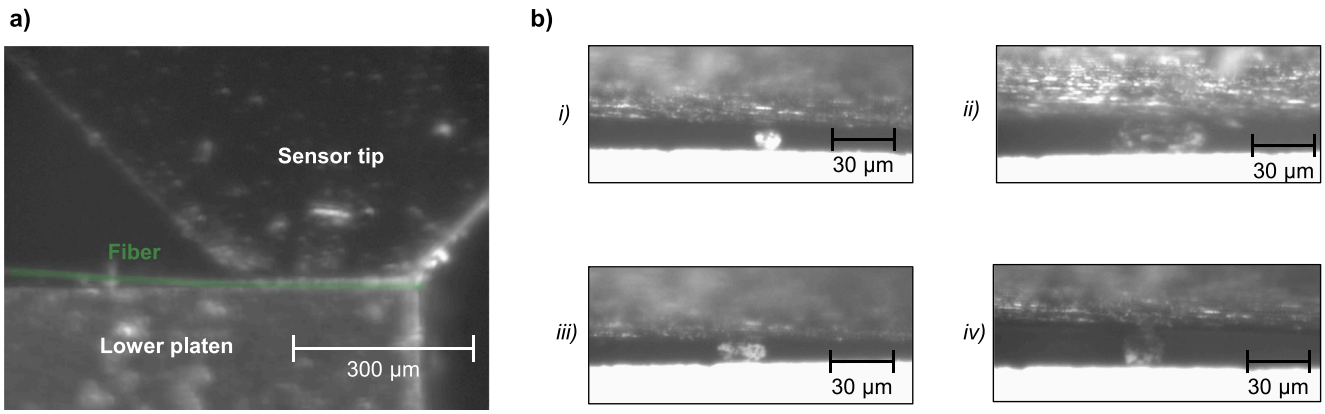

Fig. 1. a) longitudinal view of the SFTCT. a green overlay is added on the image to enhance fiber visibility. b) Transverse view of the SFTCT for: i) K29, ii) nettle, iii) hemp and iv) flax fibers. The sensor's tip can be seen on top in grey. The lower platen reflects light and appears as bright white on the bottom. Fibers can be seen in between the two platens.

2.2.2. Fiber preloading

Single fibers are placed inside the setup in a free-clamped configuration as seen in [28]. The tab-side is taped on a fixed substrate with their free end resting on a tungsten carbide lower compression platen with a roughness of 390 nm (mean arithmetic surface height). The force–displacement sensor is placed above the fiber and lowered. As discussed in [30], as the sensor gets in contact with the fiber, three distinct steps occur: i) a rigid body movement step, where the fiber slides or moves without deforming as it is being pushed by the sensor, ii) a partial compression step, where the fiber is in contact with both the sensor and lower platen and slides and rotates as it is being restricted, iii) the full fiber compression, where the fiber is completely restricted between the sensor and the lower platen and is being compressed transversely. The applied force remains around zero until the partial compression step is reached and increases significantly during full compression. To establish a full transverse compression regime, that is in accordance with the analytical models of SFTCTs, the user slowly moves the sensor against the fiber while monitoring fiber movement with the microscopes as well as the applied force. Once it is assessed that the fiber has entered a full compression regime, fiber preloading is completed.

2.2.3. SFTCT loading protocol

The loading protocol used in the SFTCT of the prepared fibers is shown in Fig. 2. The protocol aims at producing a fiber response that is as close to purely elastic as possible, allowing for the identification of an apparent fiber transverse elastic modulus, E_T. Its Repeated Progressive Loading (RPL) nature also enables the study of inelastic phenomena.

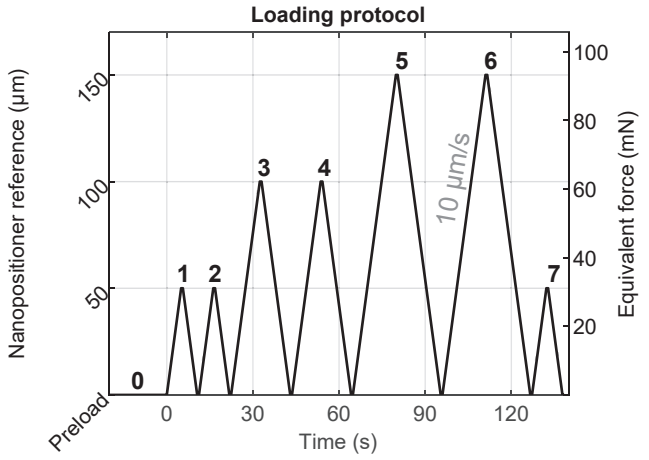

Fig. 2. Repeated Progressive Loading (RPL) protocol for SFTCTs controlled through nanopositioner generated displacement. Equivalent force levels are given on the right.

Position-controlled loading was performed through the nanopositioner that moves the force–displacement sensor. However, the sensor is a compliant structure that deforms as it compresses the fiber. Consequently, the imposed displacement has an equivalent force, equal to the sensor's compaction multiplied by its stiffness.

To prevent fiducial marker measurement uncertainties that are related to thermal drifts [31], the overall testing time is kept short at 140 s. A loading and unloading speed of 10 μm/s is used. This loading speed is shown to limit the effect of time-dependent mechanisms on fiber behavior and subsequent E_T identification (see 3.1.2) while allowing a significant amount of data acquisition at a sampling time of 0.2 s.

The test starts with an initial rest of 20 s (stage 0), allowing all setup components to load and start registering data. Seven loading and unloading cycles then take place. Multiple load levels are used to obtain results at different deformation ranges. Lower levels of loading are more likely to be close to an elastic regime at the expanse of some measurement accuracy due to the smaller fiber displacement. For higher load levels, measurements can be more precise as fiber displacement gets larger, the activation of inelastic fiber behavior is however, more likely.

Multiple loading levels also allow the study of fiber irreversible behavior as a function of applied load. Furthermore, repeating a loading cycle at the same level as the first occurrence (cycles 2, 4 and 6) allows for a study of material accommodation. Finally, a cycle of the same level as the firsts (cycle 7) is performed at the end of the protocol to study the effect of loading history on the fiber.

2.3. Transverse elastic property identification

The identification of a fiber's transverse elastic modulus, E_T, was made by inverse method using the SFTCT analytical model proposed by Jawad et al. [16]. As it will be shown in the results section of this paper, plant fibers are highly anisotropic, since their longitudinal elastic modulus greatly surpasses their transverse modulus ($E_L \gg E_T$), which simplifies some of the model's terms. Considering this simplification and the elliptical geometry approximation presented in [23], the model can be written as:

$$U = \frac{4F_L}{\pi}\left[\frac{1}{E_T}\left(sinh^{-1}\left(\frac{r}{b}\right)+ln(2)\right)-\frac{1}{2E_T}\left(1-\nu_{TT}^2\right)-\frac{\nu_{TT}}{E_T}\frac{r}{b}\left(\sqrt{1+\left(\frac{r}{b}\right)^2}-\frac{r}{b}\right)\right] \quad (1)$$

with the contact half-width b being calculated with:

$$b = \sqrt{\frac{4F_L R}{\pi E_T}} \tag{2}$$

where: U: the fiber displacement, F_L: the force per unit length, R and r: the fiber's major and minor radius respectively, E_T : the fiber's transverse elastic modulus and ν_{TT}: the Poisson ratio in the transverse plane. This formulation considers that the fiber's major axis is parallel to the platens and its minor axis is in the direction of compression, which is the most common configuration after the completion of the partial compression step (see Fig. 1,b). The user validates that the fiber is in this configuration, using the setup microscopes.

Major and minor radii values correspond to half of the mean maximum and mean minimum apparent diameter of each fiber, respectively. In the case of K29 the single average radius, measured for each fiber, is used throughout the entire model. The model assumes plane strain conditions, valid when the fiber length is significantly larger than its radius ($L \gg r$). Experimentally, the sensor tip compresses a fiber length of 300 μm while the minor radius of plant fibers and the radius of Kevlar fibers is on average in the order of 5 μm (see diameters measurements in Table 1), the hypothesis is thus satisfied.

Using the analytical model, the fiber's transverse elastic modulus is identified by inverse method through least-squares regression. A trust region algorithm is used. Force per unit length and displacement data are provided along with fiber radii values. Since ν_{TT} has a very limited impact on fiber behavior and E_T identification [13,28], it is arbitrarily set at 0.07. To establish an initial point in the identification procedure tailored to each fiber, a linear regression is conducted on the $F_L - U$ data. The quotient of the slope of this linear regression is designated as the starting point for the identification process.

During the loading stages, more irreversible fiber behavior occurs compared to the unloading stages (see 3.2). Partial compression is most likely to occur during loading, since the operator is limited by the precision of the microscopes in the preloading stage, compared to the unloading stage where the fiber has compacted to some extent. For these reasons, E_T identifications are made using the unloading stage of each cycle.

2.4. Inelastic material behavior finite element analysis

To assess how time-dependent and inelastic material behaviors of the fiber wall affect SFTCT results, FEA is employed. The FEM adheres to the geometric assumptions of the analytical model, employing a 2D, plane strain model with a circular fiber compressed between rigid and parallel platens. A linear strain formulation is used to match the infinitesimal strain approach made by the analytical model. The fiber is considered transversely isotropic. No lumen is modeled, the fiber is thus full. Any difference between analytical and finite element model results can thus be attributed to the difference in material behavior.

Given the geometric symmetry of the problem, a quarter of the fiber and half of the upper compression platen are modeled. An augmented Lagrangian formulation is used to model the contact between the two. A vertical displacement of 1 μm is imposed on the platen. The fiber's radius, R, is set at 16 μm and its transverse elastic modulus, E_T, at 1 GPa. Further details on the used FEM can be found in [23].

To comprehensively study the effect of time-dependent and inelastic behaviors, simple one parameter models are preferred, over complex counterparts with numerous, often experimentally undetermined, parameters [32]. While these simple models do not precisely capture the complexity of plant fibers behavior, they do provide a means to phenomenologically reproduce a broad spectrum of fiber behaviors that is not purely elastic, through the variation of a single parameter. A purely elastic model is also studied as a reference.

Irreversible behavior is studied by considering the fiber as a perfectly plastic material with a yield stress noted σ_Y. A von Mises yield criterion is used. The yield stress is varied to obtain values of the σ_Y/E_T ratio from 10^{-3} to 1.

Time-dependent behavior is studied through the simplest viscoelastic model, the combination of a spring of stiffness E_T and a damper with a relaxation time of τ. Since the simulation is performed by means of imposed displacement, the Maxwell model (linear combination of spring and damper), typically used in relaxation tests where strain is imposed, is chosen. The displacement speed of the platen is identical to the experimental one at 10 μm/s. For the imposed displacement of 1 μm, the overall testing duration is thus of $dt = 0.1\ s$. The relaxation time is varied to obtain values of the τ/dt ratio from 0.1 to 10^5.

Simulation force and displacement data are used to identify through least-squares regression, an apparent transverse elastic modulus E_T^{app} using the analytical model. The effect of the viscous and plastic parameters on the least-squares regression and identified transverse elastic modulus values are evaluated as outlined in [23]. The apparent modulus is compared to the fiber transverse elastic modulus defined in the simulation, E_T, through their relative difference.

$$\Delta E_T = \frac{E_T^{app} - E_T}{E_T} \tag{3}$$

Furthermore, an average least-squares regression residual ρ, is calculated as in [23], to evaluate how close the analytical model reproduces the simulated behavior.

3. Results and discussions

3.1. Finite element analysis

3.1.1. Force-displacement results and E_T identification

Fig. 3 illustrates the force per unit length F_L as function of fiber displacement U for the FEA performed for viscoelastic and elastoplastic fiber behaviors. Each curve represents a different ratio of τ/dt and σ_Y/E_T. As these ratios decrease, fiber behavior deviates significantly from the purely elastic case. Force levels decrease substantially and an inversion in non-linearity occurs from convex to concave.

These changes in fiber behavior have an impact on the value of the identified transverse elastic modulus, measured through ΔE_T and the quality of the fit of the analytical model on the FEA data, measured through ρ. The evolution of these metrics as a function of the τ/dt and σ_Y/E_T ratios is shown in Fig. 4. The reduction of force levels due to inelastic behavior makes the fiber appear less stiff. As a result, the values of the fiber's apparent transverse elastic modulii, identified using the analytical model, are lower than the fiber's actual modulus, leading to negative values of ΔE_T. The changes in the non-linearity of fiber behavior lead to increases in the value of the average least-squares regression ρ, as the analytical model does not fit as well to the FEA data.

In the case of the viscoelastic simulation, fiber behavior remains essentially identical to the purely elastic case as long as $\tau/dt \geq 100$ (see Fig. 3.a). Fiber behavior becomes almost linear at $\tau/dt = 1$ and a significant decrease in force level occurs. After the value of the ratio goes under 1, the inversion of the non-linearity in the fiber's behavior occurs leading to major changes in ΔE_T and ρ. For $\tau/dt = 0.1$ ΔE_T and ρ values reach −75 % and 36 nm (or 3.6 % of the imposed displacement) respectively.

In the case of the elastoplastic simulations, fiber behavior remains essentially identical to a purely elastic behavior until $\sigma_Y/E_T = 0.05$ (as seen in Fig. 3.b). As the ratio goes under 0.05, the inversion in non-linearity occurs, causing a major change in ΔE_T and ρ values (as seen in Fig. 4.b). These changes become more important as the σ_Y/E_T ratio decreases. For $\sigma_Y/E_T = 10^{-3}$ ΔE_T and ρ values reach −91 % and 39 nm (or 3.9 % of the imposed displacement) respectively.

3.1.2. Discussion

The aforementioned FEA results can inform experimental choices and contribute to an improved interpretation of SFTCT results for the

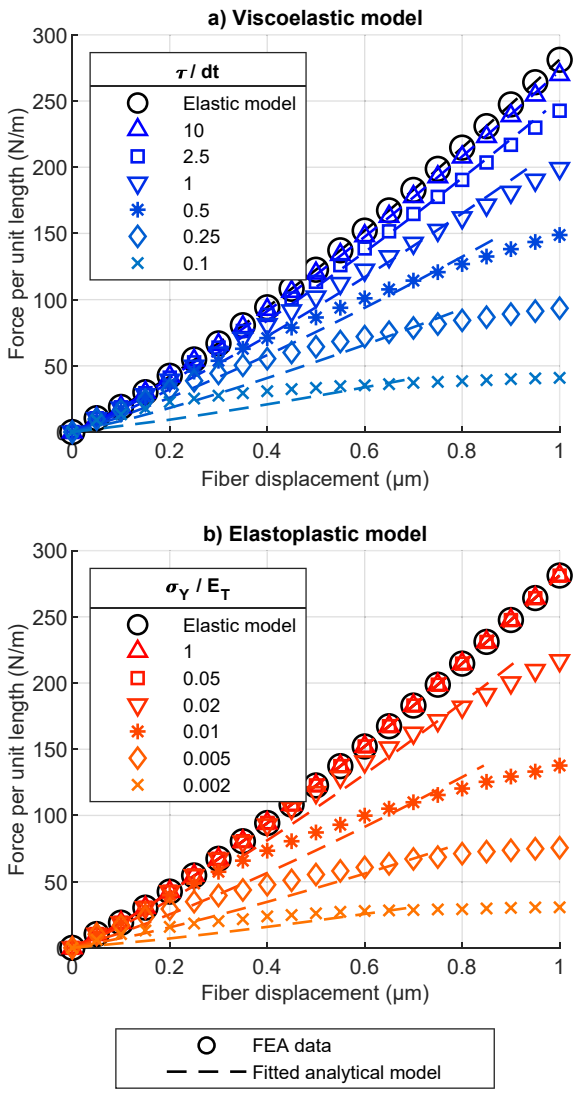

Fig. 3. FEA force per unit length and fiber displacement results for: a) viscoelastic and b) elastoplastic fiber behavior. FEA analysis is represented with markers while the dotted lines represent the fitted analytical model.

purpose of an apparent transverse elastic modulus identification.

The viscoelastic SFTCT simulations show that viscous behavior becomes predominant if relaxation times become shorter than the loading duration ($\tau < dt$). This allows viscous mechanisms to significantly affect fiber behavior, inverting its non-linearity and causing existing SFTCT analytical models, which assume purely elastic behavior, to underestimate the transverse elastic modulus ($\Delta E_T < 0$). If relaxation times are longer than loading durations ($\tau > dt$), viscous behavior has not enough time to express and no significant change in fiber behavior occurs. As a result, analytical model predictions remain accurate. While the relaxation time of plant fibers have never been characterized in the transverse plane, creep tests in the tensile direction on hemp fibers resulted in times in the order of 100 s [33]. Assuming that relaxation times in the transverse plane are of the same order of magnitude as in tensile one, loading duration should be kept in the order 100 s at most, to prevent a reversal in behavior non-linearity and limit the influence of viscous mechanisms on fiber behavior.

Experimentally, the chosen loading speed of 10 μm/s leads to, overall testing time is of 140 s (see Fig. 2). Viscous fiber behavior could thus influence the later stages of the SFTCT. However, individual loading and unloading stages last 5, 10 or 15 s depending on the compression cycle. The influence of viscous behavior on an individual loading and unloading stage should thus be limited.

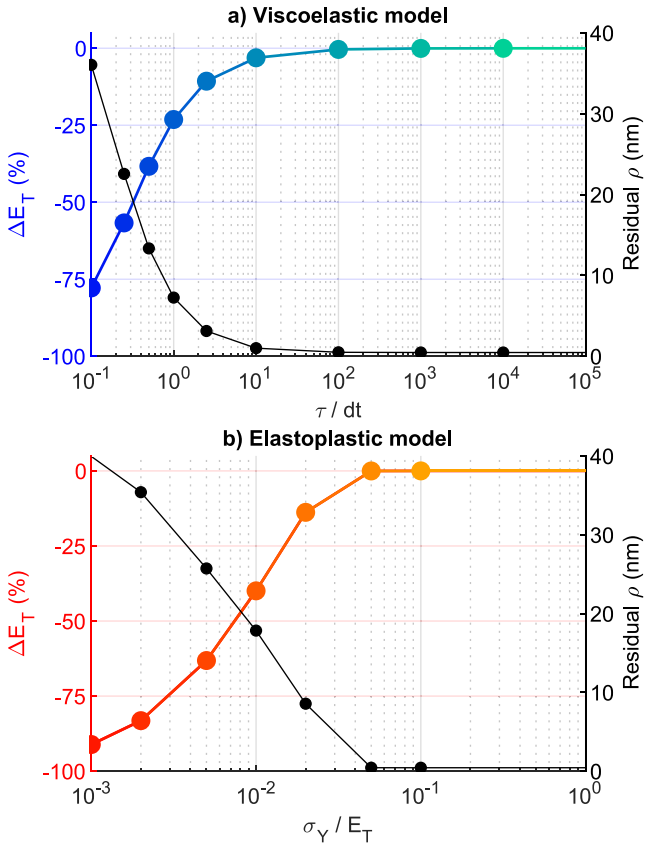

Fig. 4. Difference between actual and apparent fiber transverse elastic modulus ΔE_T and average least-squares residual ρ values for: a) viscoelastic and b) elastoplastic simulations.

The elastoplastic SFTCT simulations show that, if fibers undergo irreversible deformation during SFTCT, non-linearity inversion occurs, leading to an underestimation of the transverse elastic modulus ($\Delta E_T < 0$). Consequently, assuming that loading speeds are adapted to minimize the effects of time-dependent mechanisms on fiber behavior, force–displacement SFTCT results exhibiting an inversed non-reality point to irreversible mechanisms taking place, rendering such data unsuitable for the identification of an apparent transverse elastic modulus, using the purely elastic SFTCT analytical model.

3.2. Experimental testing

3.2.1. Force-displacement results

Fig. 5 shows the force–displacement results of the transverse compression for the 5 tested fibers of each of the 4 fiber types. Fig. 6 presents these results for individual fibers. A few key characteristics can be observed:

- For each compression cycle, an open hysteresis loop occurs with the fiber's displacement not returning to its initial value. Inelastic phenomena thus clearly take place for all tested fibers. The surface of a given hysteresis loop is more important at the first occurrence of a given loading level compared to the second one.
- The surface of these hysteresis loops is much greater in the case of the plant fibers compared to the one for K29 fibers. Inelastic behavior is thus more prevalent in plant fibers for the tested loading levels.
- The convex non-linearity in the unloading stage of the compression cycle matches analytical model predictions. The concave non-linearity during the loading stage does not. As seen previously with FEA, this concave response can be a result of the inelastic or time-

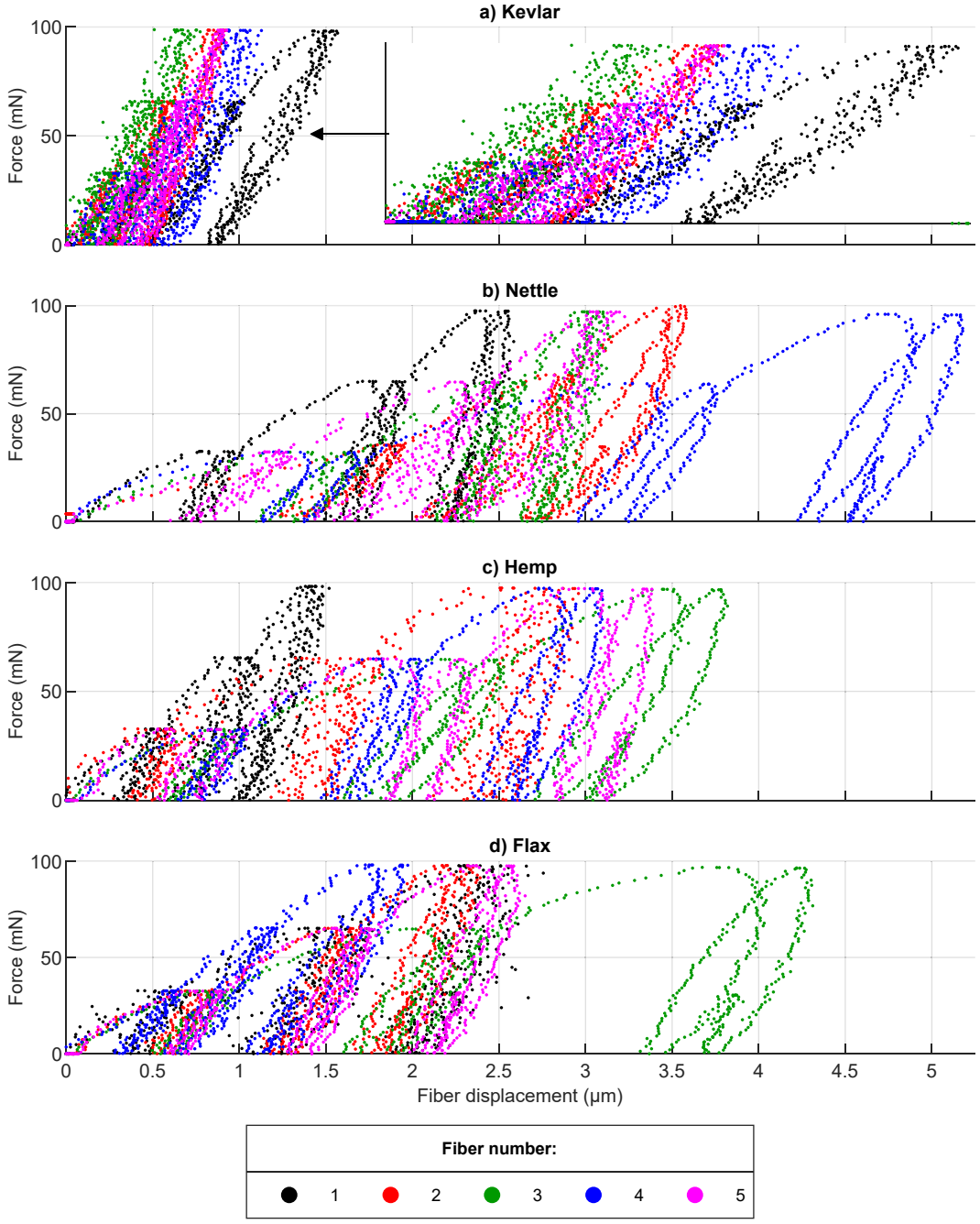

Fig. 5. SFTCT force–displacement results for: a) Kevlar (K29), b) nettle, c) hemp and d) flax fibers.

dependent behavior of the fiber wall material. Given the short loading duration, irreversible phenomena are more likely to cause this change in non-linearity rather than time dependent ones. Inelastic behavior is thus more important during the loading stage of the compression rather than the unloading.

3.2.2. *Residual displacement*

The average difference in residual displacement between the end and the beginning of a cycle, normalized by the original fiber radius in the direction of compression (average radius for Kevlar (K29) fiber, minor radius for plant fibers), is shown in Fig. 7. These values illustrate the magnitude of the inelastic nature of fiber behavior and offers insights on its nature. For K29 fibers, residual displacement remains under 2 % of the radius while for plant fibers these values can reach up to 10 %. Regardless of fiber nature however, a clear correlation can be seen between loading cycle and residual displacement. For the first occurrence of a loading level, residual displacement is much more important than for the second one. However, higher loading levels do not necessarily result in higher residual displacements, no clear correlation between the two is apparent.

Typical irreversible inelastic material behavior could explain these results. As the fiber gets compressed for the first time at a given load level, it locally yields and deforms irreversibly, resulting in a residual displacement value. As a second loading takes place at the same force level, less yielding occurs, leading to lower residual displacement values and less important hysteresis loops in terms of surface. The open hysteresis loops could also be a result to some extent, of reversible time-dependent behavior. However, as the proposed loading protocol does not offer a recovery stage at the end of each compression cycle, to reduce overall testing time. Thus, the extent of reversible inelastic behavior

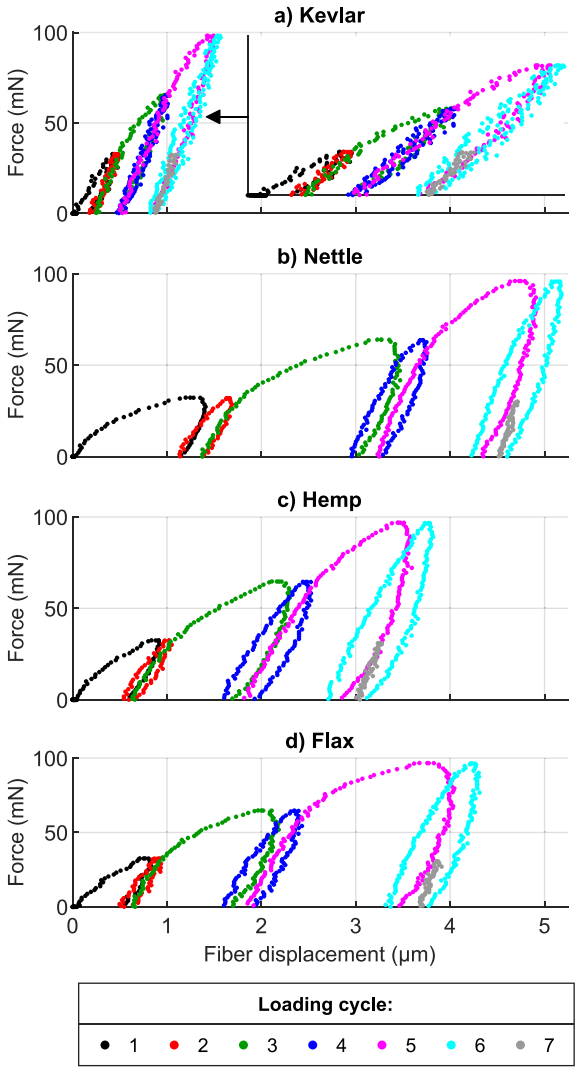

Fig. 6. SFTCT individual fiber force–displacement results for: a) Kevlar (K29) fiber n ° 3, b) nettle fiber n ° 4, c) hemp fiber n ° 3 and d) flax fiber n ° 3.

cannot be quantified.

Irreversible fiber behavior may also result from structural effects as discussed in [23]. In the case of plant fibers, the lumen could have such an effect. During the loading stage, significant fiber displacement could be attributed to the compaction of its lumen (see Fig. 8.b). If the lumen compacts irreversibly and does not come back to its original position, significantly less displacement would occur during the unloading stage. Furthermore, as the loading level is repeated for the next cycle, the irreversibly deformed lumen does not compact as much, leading to lower displacement values and smaller hysteresis loop surfaces (see Fig. 8.c). When a higher load is applied in next compression cycle, further compaction occurs, leading once again to high residual displacement (see Fig. 8.d). In the case of K29, small porosities and an outer skin have been reported [13] which must lead to structural mechanisms that lead to changes in fiber behavior. However, their size is small compared to plant fiber lumens and their effect should thus be minor in comparison. This compaction mechanism could thus explain why displacements during the loading stage are significantly more important for plant fibers compared to K29 fibers.

3.2.3. *Apparent transverse elastic properties*

As discussed in the previous sections, the unloading stages of the SFTCT experimental protocol are better suited for the identification of an apparent transverse elastic modulus since they show limited signs of inelastic behavior while also being less likely to produce partial fiber compression movements. For this reason, the unloading stages are isolated, and the identification procedure is only performed on them. Fig. 9 shows the fitted analytical model over force and displacement data, for all fibers at the unloading stage of the sixth cycle. Displacements at the unloading stage are very small (under 1 μm) which leads to some noise in the data in the case of a few fibers. However, in the majority of cases, the analytical model fits well over the experimental data.

Fig. 10 illustrates the average apparent transverse elastic modulus for each fiber type, identified at a given unloading stage. An asterisk marks cases where the average was based on 4 fiber unloads because one fiber's least-squares identification returned the starting point value. The apparent modulus of K29 fibers is identified between 1.6 and 2.9 GPa which is consistent with the values reported in the literature [7,13,18]. The apparent modulus of plant fibers is of the same order of magnitude as the K29 fibers, with no fiber type showing a distinct difference. Nevertheless, the variations observed for plant fibers are larger. This can be attributed in part to the inherent variability of plant fibers due to their biological nature and thigmomorphogenesis [1]. Some cases of

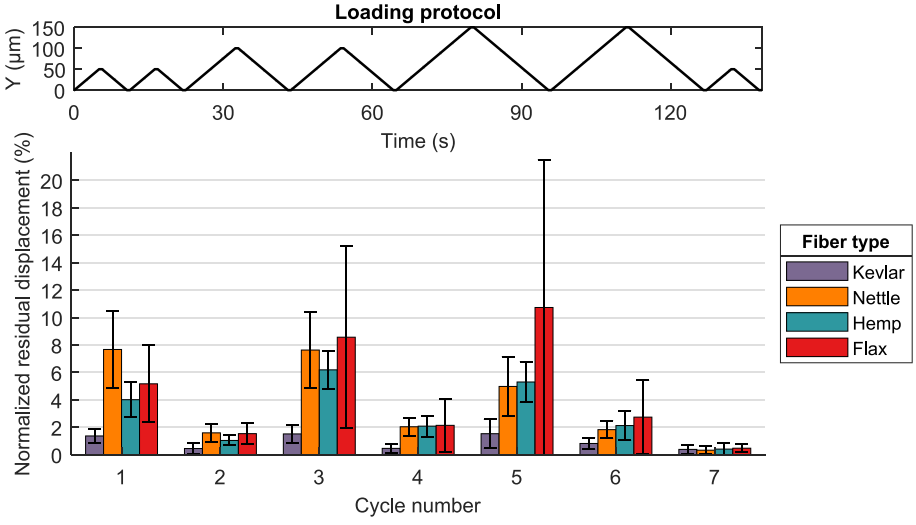

Fig. 7. Average normalized residual displacement for each fiber type at a given compression cycle. Large variations are results of significant differences in diameter and residual displacement of a single fiber.

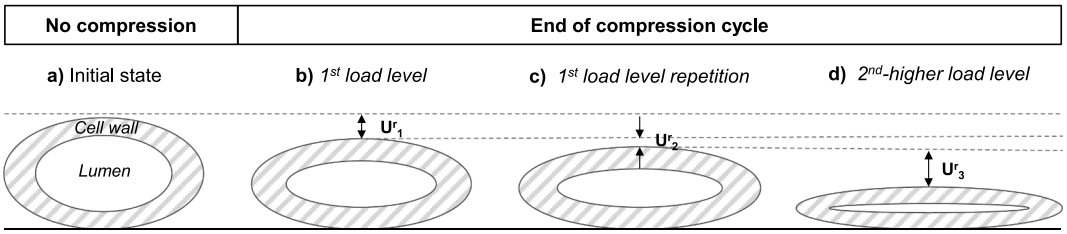

Fig. 8. Illustration of fiber residual displacement (U^r) related to lumen compaction during SFTCT. Displacement are depicted as much larger than the experimental levels for visual clarity.

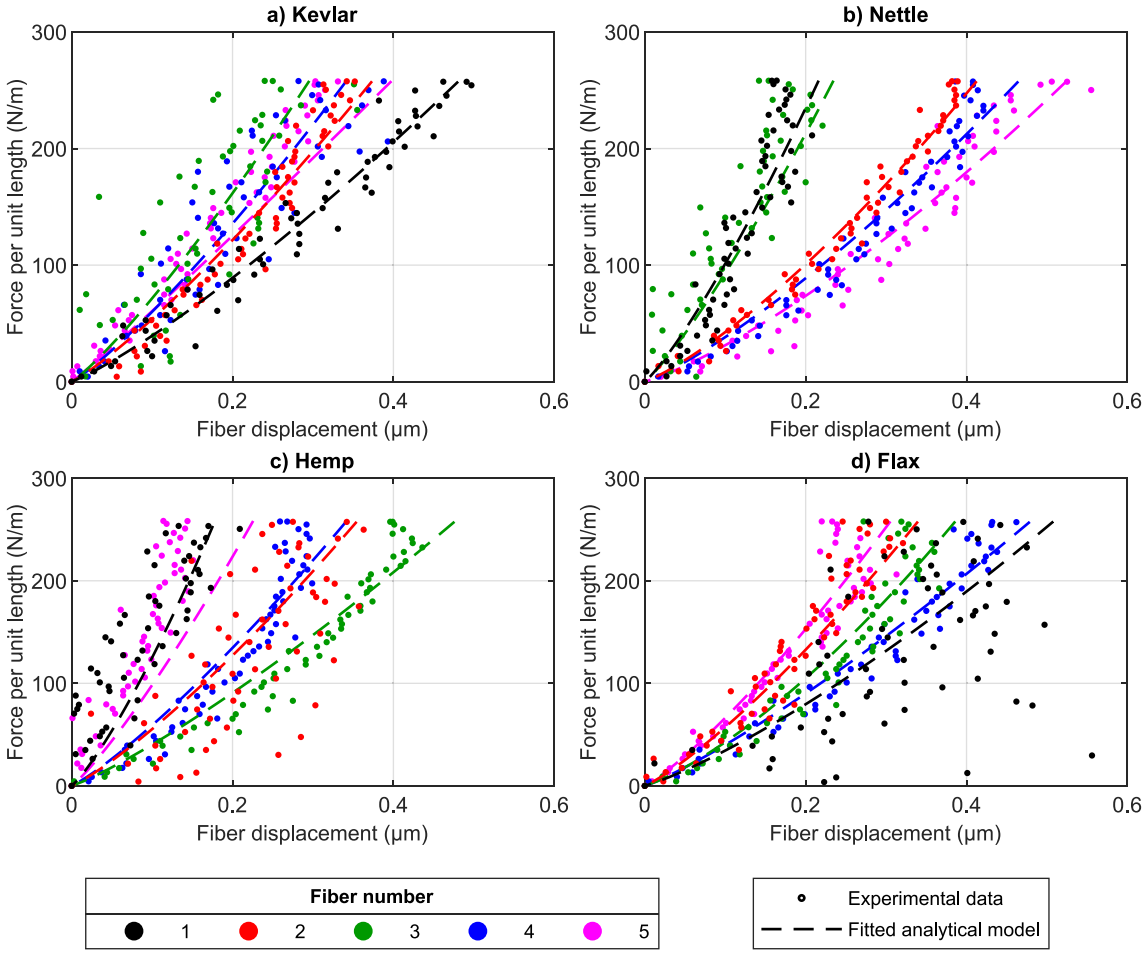

Fig. 9. SFTCT force per unit length-displacement results at the unloading stage of cycle 6 for: a) K29, b) nettle, c) hemp and d) flax fibers. The fitted analytical model is represented with dotted lines. Fiber displacements values are offset to start at 0, facilitating comparisons between fibers.

higher noise in plant fiber displacement measurement, as in Fig. 9.d also contribute to these variations.

A positive correlation between loading level and apparent modulus is quite apparent for all tested fibers. This correlation has not been observed on other fiber types tested on the same setup, making it unlikely to be caused by an external factor. The apparent moduli identified at the first occurrence of a given load level and its repetition, are very similar. When the load level increases however (cycle 3 and 5), so does the value of the apparent modulus. When the load is decreased in cycle 7, at the same level as cycles 1 and 2, the apparent modulus decreases as well to comparable, albeit slightly higher levels.

Once again, both material and structural mechanisms could explain this increase in fiber apparent stiffness. Material irreversible mechanisms, expressed during the compression's loading stage, could have a hardening effect. Regarding structural mechanisms, as the fiber gets more irreversibly compressed, a flattened section will be created where contact with the platens occurs, and a more elliptical and flat shape will be adopted in general. Such changes in geometry have been shown to lead to an increase in apparent stiffness when not actively accounted for in the analytical model [23]. In the case of plant fibers, irreversible lumen compaction could also have an effect. The compaction of the lumen adds a structural displacement to the material deformation of the fiber, leading to a decrease in apparent stiffness [23]. If the lumen collapses irreversibly to some extent during the loading stage, some of this structural displacement is lost, leading to an increase in apparent stiffness. All described mechanisms should become more important as the loading level increases and have a diminished impact if the loading level remains the same.

In the case of cycle 7, where a decrease in load occurs, none of the previously proposed material and structural mechanisms take place.

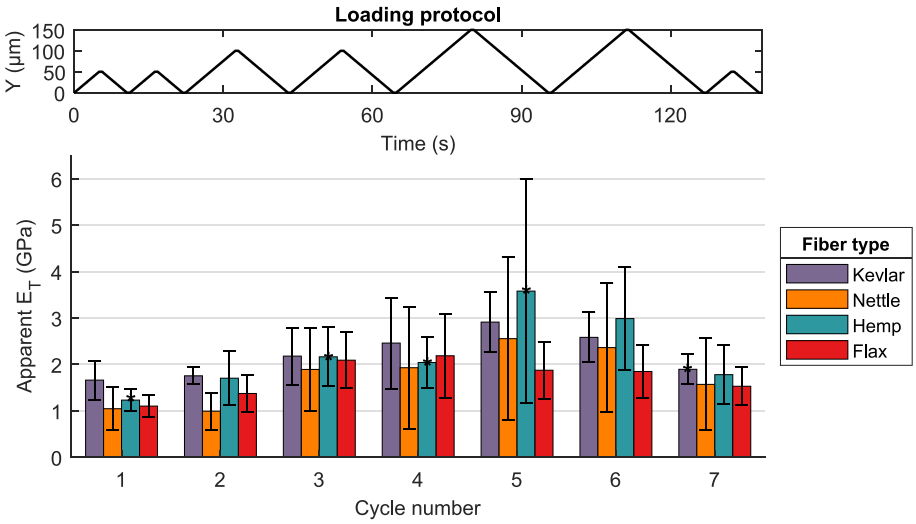

Fig. 10. Average apparent transverse elastic modulus for each fiber type, identified at the unloading stage of each compression cycle. An asterisk marks cases where the average is based on 4 fibers due to identification issues with one fiber.

However, apparent stiffness does not stay the same but decreases instead. This decrease points to potential fiber damage or softening mechanisms that would lead to a decrease in apparent stiffness. Such softening mechanisms could only become apparent when load levels decrease and the mechanisms causing an apparent stiffness increase are absent. Nevertheless, the apparent stiffness for cycle 7 is slightly higher than the one identified at cycles 1 and 2, which are performed with the same loading amplitude. Changes in fiber geometry induced by the previous loading cycles can explain this difference. At cycle 7 an increase in fiber ellipticity and flatness should occur along with some lumen compaction compared to cycles 1 and 2, leading to an increased apparent stiffness.

3.2.4. Discussion

Table 2 presents the average value of the apparent transverse elastic modulus for all fibers across all unloading stages. Given the values of the standard deviations, the 4 fibers present similar apparent transverse stiffness at approximatively 2 GPa. Values of longitudinal modulii E_L, taken from available literature, are also presented. When comparing E_T and E_L it becomes clear that plant fibers are highly anisotropic materials. Flax and nettle fibers have a E_L/E_T ratio of 20 to 44 which is comparable to K29 fibers. Hemp is less anisotropic with a ratio between 6 and 20.

In the case of flax fibers, the apparent modulus identified in this work is significantly different from the value indirectly identified by Baley el al. [5] with tests at the composite scale at around 8 GPa. While indirect testing methods come with a series hypotheses (perfect fiber–matrix interface, uniform fiber properties, geometries and distribution in matrix, etc.) that can justify at least some of these differences [4], the increased apparent fiber stiffness in the composites could be a result of other mechanisms too. For one, fibers are not free to deform transversely when incorporated in the composite, since the matrix significantly limits such deformations. This could lead to an increase in apparent fiber stiffness. Furthermore, the flax fibers must have been subject to important transverse stresses, during fiber processing and composite compression molding, which as discussed previously could also lead to an increase in apparent fiber stiffness. Finally, resin diffusion within the fiber lumen or cell wall could also lead to such an increase.

These results highlight the complexity of plant fiber transverse behavior. When considered for structural applications, the mechanisms that could lead to potential increases or decreases in apparent fiber transverse elastic stiffness should be carefully considered, since they could cause a significant change in the fiber and subsequently composite, mechanical properties.

Table 2
Average apparent transverse elastic across all unloading stages for each fiber type. Anisotropy ratios E_L/E_T are calculated by using longitudinal modulii values available in the literature.

Fiber	Kevlar®29	Nettle	Hemp	Flax
E_T(GPa)	2.21 ± 0.47	1.76 ± 0.60	2.21 ± 0.81	1.71 ± 0.39
E_L(GPa)	84 [34]	37–75 [35]	14–44 [1]	36–79 [1]
E_L/E_T	38	20–44	6–20	22–44

4. Conclusions

In this paper, SFTCTs were performed experimentally for the first time on flax, hemp and nettle fibers. As a precursor to these tests, FEA was employed to investigate the impact of time-dependent mechanisms and fiber wall material inelasticity on fiber behavior. Both viscous and plastic behaviors were shown to produce a reversal in the non-linearity of fiber behavior, from convex to concave. However, the influence of viscous behavior was shown to be minimal if an appropriate loading speed is used. Such non-linearity inversions were observed experimentally during the loading stage; therefore, plant fiber apparent elastic moduli were identified during the unloading stage, where analytical predictions were met.

An RPL was used to identify the apparent transverse elastic moduli of the fibers while also revealing their inelastic behavior. The apparent transverse elastic moduli of plant fibers were found to be similar to those of K29 fibers, ranging from 1 to 3 GPa. Comparing these moduli to the longitudinal ones available in the literature showed that plant fibers are highly anisotropic materials, with E_L/E_T ratios of 6 to 20 for hemp and 20 to 40 for flax and nettle.

Inelastic behavior was significantly more pronounced in plant fibers compared to K29 fibers. This behavior can be attributed to material causes related to fiber composition and ultrastructure, as well as structural effects, notably lumen compaction. These material and structural effects influence the identified apparent transverse elastic modulus, which positively correlates with the load level. Consequently, loading history can significantly affect plant fiber transverse properties.

These findings offer valuable insights for the PFC community. Accurate knowledge of the plant fiber transverse properties aids in predicting and optimizing PFC behavior under various loading conditions. Understanding the highly anisotropic nature of plant fibers allows for their more efficient use in PFCs through tailored placement and orientation. Insights on the effect of loading history on fiber behavior can also

inform improvements in plant fiber processing and PFC manufacturing. Overall, these findings can contribute to the expansion of PFCs to more demanding applications, accelerating the transition towards more sustainable composite materials.

Future research using the proposed experimental setup can further improve the understanding of plant fiber transverse behavior. The influence of relative humidity on fiber behavior can be studied. Higher loads could be applied in tandem with advanced imaging techniques to study lumen compaction, compressive failure, and damage mechanisms. Finally, integrating fine temperature control inside the testing chamber would enable long-term experimental endeavors such as creep or fatigue tests, facilitating the characterization of further plant fiber transverse properties.

CRediT authorship contribution statement

Jason Govilas: Writing – review & editing, Writing – original draft, Visualization, Software, Methodology, Investigation. **Anouk Chevallier:** Writing – review & editing, Visualization, Methodology, Investigation. **Wajih Akleh:** Writing – review & editing, Methodology, Investigation. **Johnny Beaugrand:** Writing – review & editing, Supervision, Conceptualization. **Cédric Clévy:** Writing – review & editing, Supervision, Funding acquisition, Conceptualization. **Vincent Placet:** Writing – review & editing, Supervision, Funding acquisition, Conceptualization.

Declaration of competing interest

The authors declare that they have no known competing financial interests or personal relationships that could have appeared to influence the work reported in this paper.

Data availability

Data will be made available on request.

Acknowledgements

These works have been supported by the European Union's Horizon 2020 research and innovation program under grant agreement No 771134. The project NETFIB was carried out under the ERA-NET Cofund SusCrop (Grant N°771134), being part of the Joint Programming Initiative on Agriculture, Food Security and Climate Change (FACCE-JPI). This work has also been supported by EIPHI Graduate School under ("ANR-17-EURE-0002"), the French RENATECH network through its FEMTO-ST technological facilities MIMENTO as well as the French ROBOTEX network (TIRREX ANR-21-ESRE-0015) and its FEMTO-ST technological facility CMNR. Special thanks to Dr. Sébastien Joannés of Ecole des Mines de Paris – Université PSL for providing the Kevlar®29 fibers and Pr. Jörg Müssig, Jonas Baumann and Lea Bothe of HSB—City University of Applied Sciences Bremen, for their extensive work on nettle fiber preparation. Authors also acknowledge Joel Agnus, Patrick Rougeot and Pr. Nicolas Martin for their help and involvement in this work.

References

[1] Bourmaud A, Beaugrand J, Shah DU, Placet V, Baley C. Towards the design of high-performance plant fibre composites. Prog Mater Sci 2018;97:347–408. https://doi.org/10.1016/j.pmatsci.2018.05.005.
[2] Zimniewska M, Wladyka-przybylak M, Mankowski J. Cellulose fibers: bio- and nano-polymer composites. Cellulose Fibers: Bio- and Nano-Polymer Composites 2011. https://doi.org/10.1007/978-3-642-17370-7.
[3] Peças P, Carvalho H, Salman H, Leite M. Natural fibre composites and their applications: a review. J Composites Sci 2018;2:1–20. https://doi.org/10.3390/jcs2040066.
[4] Shah DU, Nag RK, Clifford MJ. Why do we observe significant differences between measured and 'back-calculated' properties of natural fibres? Cellul 2016;23:1481–90. https://doi.org/10.1007/s10570-016-0926-x.
[5] Baley C, Perrot Y, Busnel F, Guezenoc H, Davies P. Transverse tensile behaviour of unidirectional plies reinforced with flax fibres. Mater Lett 2006;60:2984–7. https://doi.org/10.1016/j.matlet.2006.02.028.
[6] Comas-Cardona S, Le Grognec P, Binetruy C, Krawczak P. Unidirectional compression of fibre reinforcements. Part 1: a non-linear elastic-plastic behaviour. Compos Sci Technol 2007;67:507–14. https://doi.org/10.1016/j.compscitech.2006.08.017.
[7] Kawabata S. Measurement of the transverse mechanical properties of high-performance fibres. J Text Inst 1990;81:432–47. https://doi.org/10.1080/00405009008658721.
[8] Lim J, Zheng JQ, Masters K, Chen WW. Mechanical behavior of A265 single fibers. J Mater Sci 2010;45:652–61. https://doi.org/10.1007/s10853-009-3979-5.
[9] Naito K, Tanaka Y, Yang JM. Transverse compressive properties of polyacrylonitrile (PAN)-based and pitch-based single carbon fibers. Carbon 2017;118:168–83. https://doi.org/10.1016/j.carbon.2017.03.031.
[10] Phoenix S, Skelton J. Transverse compressive moduli and yield behavior of some orthotropic, high-modulus filaments. Text Res J 1974:934–40. https://doi.org/10.1177/004051757404401203.
[11] Singletary J, Davis H, Song Y, Ramasubramanian MK, Knoff W. Transverse compression of PPTA fibers. Part I. fiber transverse structure. J Mater Sci 2000;35:583–92. https://doi.org/10.1023/A:1004716108638.
[12] Cheng M, Chen W, Weerasooriya T. Experimental investigation of the transverse mechanical properties of a single Kevlar® KM2 fiber. Int J Solids Struct 2004;41:6215–32. https://doi.org/10.1016/j.ijsolstr.2004.05.016.
[13] Wollbrett-Blitz J, Joannès S, Bruant R, Le Clerc C, De La Osa MR, Bunsell A, et al. Multiaxial mechanical behavior of aramid fibers and identification of skin/core structure from single fiber transverse compression testing. J Polym Sci B 2016;54:374–84. https://doi.org/10.1002/polb.23763.
[14] Sockalingam S, Bremble R, Gillespie JW, Keefe M. Transverse compression behavior of Kevlar KM2 single fiber. Compos A Appl Sci Manuf 2016;81:271–81. https://doi.org/10.1016/j.compositesa.2015.11.032.
[15] Guo Z, Casem D, Hudspeth M, Nie X, Sun J, Chen W. Transverse compression of two high-performance ballistic fibers. Text Res J 2016;86:502–11. https://doi.org/10.1177/0040517515592814.
[16] Jawad SA, Ward IM. The transverse compression of oriented nylon and polyethylene extrudates. J Mater Sci 1978;13:1381–7. https://doi.org/10.1007/BF00553190.
[17] Kotani T, Sweeney J, Ward IM. The measurement of transverse mechanical properties of polymer fibres. J Mater Sci 1994;29:5551–8. https://doi.org/10.1007/BF00349946.
[18] Jones MCG, Lara-Curzio E, Kopper A, Martin DC. The lateral deformation of cross-linkable PPXTA fibres. J Mater Sci 1997;32:2855–71. https://doi.org/10.1023/A:1018672400459.
[19] Stamoulis G, Wagner-Kocher C, Renner M. Experimental study of the transverse mechanical properties of polyamide 6.6 monofilaments. J Mater Sci 2007;42:4441–50. https://doi.org/10.1007/s10853-006-0655-x.
[20] Mikczinski M, Nguyen HX. Assessing transverse fibre properties : fibre compression and artificial hornification by periodic compression. Adv Pulp and Paper Res, Trans XVth Fundamental Research Symposium, Cambridge 2013:803–20. https://doi.org/10.15376/frc.2013.2.803.
[21] Placet V, Cissé O, Lamine BM. Nonlinear tensile behaviour of elementary hemp fibres. Part I: investigation of the possible origins using repeated progressive loading with in situ microscopic observations. Compos A Appl Sci Manuf 2014;56:319–27. https://doi.org/10.1016/j.compositesa.2012.11.019.
[22] Richely E, Durand S, Melelli A, Kao A, Magueresse A, Dhakal H, et al. Novel insight into the intricate shape of flax fibre lumen. Fibers 2021:9. https://doi.org/10.3390/fib9040024.
[23] Govilas J, Clévy C, Beaugrand J, Placet V. Investigating the influence of plant fiber geometry on apparent transverse elastic properties through finite element analysis. Compos A Appl Sci Manuf 2023;175:107789. https://doi.org/10.1016/j.compositesa.2023.107789.
[24] Singletary J, Davis H, Song Y, Ramasubramanian MK, Knoff W. Transverse compression of PPTA fibers. Part II. fiber transverse structure. J Mater Sci 2000;35:583–92. https://doi.org/10.1023/A:1004716108638.
[25] McDaniel PB, Sockalingam S, Deitzel JM, Gillespie JW, Keefe M, Bogetti TA, et al. The effect of fiber meso/nanostructure on the transverse compression response of ballistic fibers. Compos A Appl Sci Manuf 2017;94:133–45. https://doi.org/10.1016/j.compositesa.2016.12.003.
[26] Garat W, Corn S, Le Moigne N, Beaugrand J, Bergeret A. Analysis of the morphometric variations in natural fibres by automated laser scanning: towards an efficient and reliable assessment of the cross-sectional area. Compos A Appl Sci Manuf 2018;108:114–23. https://doi.org/10.1016/j.compositesa.2018.02.018.
[27] Roche EJ, Wolfe MS, Suna A, Avakian P. Light diffraction effects from kevlar aramid fibers. J Macromolecular Sci, Part B 1985;24:141–57. https://doi.org/10.1080/00222348508248022.
[28] Govilas J, Guicheret-Retel V, Amiot F, Beaugrand J, Placet V, Clévy C. Platen parallelism significance and control in single fiber transverse compression tests. Compos A Appl Sci Manuf 2022:159. https://doi.org/10.1016/j.compositesa.2022.106990.
[29] Laermer F, Franssila S, Sainiemi L, Kolari K. (2020) Deep reactive ion etching. INC. doi: 10.1016/B978-0-12-817786-0.00016-5.
[30] Andre AN, Lehmann O, Govilas J, Laurent GJ, Saadana H, Sandoz P, et al. Automating robotic micro-assembly of fluidic chips and single fiber compression

tests based-on $XY\Theta$ visual measurement with high-precision fiducial markers. IEEE Trans Autom Sci Eng 2022:1–14. https://doi.org/10.1109/TASE.2022.3218686.

[31] Mauze B, Dahmouche R, Clevy C, Sandoz P, Hennebelle F, Laurent GJ. Visual measurements at small scales: guidelines to reduce uncertainties down to a few nanometers. Proce MARSS 2020: Int Conference on Manipulation, Automation, and Robotics at Small Scales 2020. https://doi.org/10.1109/MARSS49294.2020.9307854.

[32] Trivaudey F, Placet V, Guicheret-Retel V, Boubakar ML. Nonlinear tensile behaviour of elementary hemp fibres. Part II: Modelling using an anisotropic viscoelastic constitutive law in a material rotating frame. Compos A Appl Sci Manuf 2015;68:346–55. https://doi.org/10.1016/j.compositesa.2014.10.020.

[33] Cisse O, Placet V, Guicheret-Retel V, Trivaudey F, Boubakar ML. Creep behaviour of single hemp fibres. Part I: viscoelastic properties and their scattering under constant climate. J Mater Sci 2015;50:1996–2006. https://doi.org/10.1007/s10853-014-8767-1.

[34] Bencomo-Cisneros JA, Tejeda-Ochoa A, García-Estrada JA, Herrera-Ramírez CA, Hurtado-Macías A, Martínez-Sánchez R, et al. Characterization of Kevlar-29 fibers by tensile tests and nanoindentation. J Alloy Compd 2012;536:S456–9. https://doi.org/10.1016/j.jallcom.2011.11.031.

[35] Jeannin T, Yung L, Evon P, Labonne L, Ouagne P, Lecourt M, et al. Native stinging nettle (Urtica dioica L.) growing spontaneously under short rotation coppice for phytomanagement of trace element contaminated soils: fibre yield, processability and quality. Ind Crop Prod 2020;145:111997. https://doi.org/10.1016/j.indcrop.2019.111997.